Methods and Results of Diagnosis in a Closed-Cycle MHD Blowdown Generator

E. M. van Veldhuizen* and H. J. Flinsenberg†
Eindhoven University of Technology, Eindhoven, the Netherlands

After many years of experimenting with the 5-MW thermal blowdown generator, much knowledge has been gained about its construction and operation. Measurements are described for obtaining useful information about the system. The most important parameters that have been determined are the density and size of dust particles, the density of impurities, seed ratio, electron temperature and density, streamer velocity, and pressure. The maximum power output that has been reached is 423 kW with an enthalpy extraction of 8.5%. The most important functional conclusions that can be drawn about the generator are 1) the hot flow train inside the magnet should not contain any metal components except for the electrodes because shortcircuiting gives a great increase in the exit pressure; 2) water contamination should be reduced to less than 100 ppm; and 3) the load resistors must have a low inductance in order to provide good ignition conditions for the streamers.

I. Introduction

RESEARCH and development of MHD generators has been mainly concerned with combustion systems (open cycle). Although the closed-cycle system is technically more complicated, it has many advantages that make its investigation worthwhile. The most important advantages are: 1) the operating temperature can be much lower than that for open-cycle generators (2000 K against 2700 K); and 2) any heat source can be used, provided that a suitable heat exchanger can be built.

The reason for the lower gas temperature is that the working gas, usually argon or sometimes helium, is atomic. In that case the electron temperature can be much higher than the gas temperature.[1] Since electrical conductivity is determined mainly by the electron temperature, this situation is favorable. In open-cycle systems, the presence of molecules prohibits this nonequilibrium situation. The energy of the electrons is easily transferred to rotations and vibrations of the molecules. It has been measured and calculated that the presence of 100 ppm CO_2 or 3000 ppm N_2 causes a power reduction of 30–40% in a closed-cycle generator operated with a shock tube.[2] The need for low molecular contamination is another technical difficulty of the closed-cycle generator but it can be achieved, as pointed out in Ref. 3, and demonstrated in the experiments.

The objective of the MHD blowdown project is to demonstrate high-enthalpy extraction on a time scale of 10–20 s. In 1975, an enthalpy extraction of 24% was reached with shock-tunnel-driven generators.[4,5] The main parameters of the experiments of Ref. 5 were a stagnation pressure of 7.5 bar, a stagnation temperature of 3400 K, a magnetic induction of 3.5 T, and a duration of 5 ms. From a series of measurements and calculations it was concluded that the blowdown generator should be able to deliver 1 MW of electrical energy at a stagnation temperature of 2000 K, a stagnation pressure of 7 bar, and a magnetic induction of 5 T. This would be an enthalpy extraction of 20%, which is almost twice as high as that obtained with fuel-burning generators.

Diagnostic methods for use with fuel-burning MHD generators have received considerable attention in literature, and a survey of these methods can be found in Ref. 6. It is surprising that very few new methods have appeared and that many of the alternatives mentioned have not yet had any success when applied to MHD flows. This suggests that problems are encountered making these measurements due to the difficulties associated with the high flow velocity (>1000 m/s), the high temperature, and the accessibility to the duct because of the magnet.

In this paper only the successful methods are discussed together with a short description of the blowdown facility. The data presented here have been limited to the most interesting cases along with a discussion of the problems encountered and conclusions that were drawn.

II. Description of the Facility

Fig. 1 shows a line diagram of the facility. In the direction of the flow the main components are, successively, the argon supply system, the regenerative heat exchanger, the high-temperature gate valve, the cesium injection system, the nozzle, the MHD generator duct with the diffusor system, and the cryogenic magnet. After the desired temperature profile has been reached across the bed of the heat exchanger, the heater is evacuated to approximately one Torr. Then the heater is filled with argon, at a pressure of 1.2 bar, until a negligible pressure differential occurs along the pressurized duct. At this point, the ceramic-lined high-temperature valve (i.d. 0.25 m) can be opened, and a programmable automatic logic controller handles the timing sequence of the run. The ball valve in the supersonic diffusor is then opened and argon is bled from the cesium injection system. The flow starts from valve V-1 upstream of the heat exchanger while a pressure control valve keeps the argon at a nominal stagnation pressure of 7 bar. Sufficient argon gas for one blowdown run is supplied from a 4-m^3 spherical tank at a pressure of 100 bar which is connected to the liquid argon storage system. After passing through the heater, an adjustable spray of cesium droplets is injected into the gas flow; the flow continues through an $M=1.6$ nozzle which accelerates the flow to approximately 1000 m/s. Then follows the generator duct, a supersonic and subsonic diffuser system. In the diffuser systems, the pressure is relieved before the argon/cesium mixture exhausts into the scrubber tank. After 30–60 s, the run is stopped by closing valve V-1, but an argon bleed through the cesium injection system is maintained in order to prevent oxidation in the generator duct. Finally, the ball valve is closed and the run is complete. The generated power is delivered to adjustable oil-immersed load resistors. More details of the components are given in Refs. 7 and 8.

Received April 17, 1986; revision received Nov. 17, 1986.

*Department of Electrical Engineering; presently with Philips Telecommunications and Data Systems, Apeldoorn, the Netherlands.
†Group Electrical Energy Systems.

III. Diagnostics

Survey

Understanding the principles of a closed-cycle MHD generator requires a considerable amount of information; however, three basic processes of the MHD energy conversion process need to be recognized in order to diagnose its operation.

1) *The plasma physical process occurring in the generator.* The ionization and excitation processes leading to the onset of a typically nonequilibrium plasma especially have to be studied in relation to the various parameters of the system, i.e., impurity level, magnetic field, cesium injection rate, stagnation temperature, external load on the generator, etc.

2) *The electrical performance of the generator.* The externally generated Faraday and Hall voltages are important together with the internal losses occurring in the vicinity of the electrodes, for instance.

3) *The gasdynamic performance of the hot flow train.* The dynamic interaction between the gas flow and the net retarding forces acting on the flow especially have to be studied, together with the onset of boundary layers.

Measurements are severely affected by certain phenomena that occur in the generator. They include the strongly heterogeneous nature of the plasma in the form of constricted discharges, the relaxation processes, and the electrode effects, which, coupled with the discharge structures, make the diagnosis very complex. The discharges move through the plane of observation with a supersonic velocity. Therefore, the measurements must be carried out with a high time resolution and at various positions.

Mie Scattering

In order to check the heat exchanger performance and to determine the influence of the dust content of the plasma on the MHD conversion process an in situ laser Mie-scattering technique has been developed. The alumina particles concentration in the gas flow and the particle diameter can be measured simultaneously. The beam of a 2-W argon-ion laser (514.5 nm) is focused to a waist of 3 mm and the scattering volume will occur in the subsonic part of the diffuser. The scattered laser light is focused on slit S2, which has an adjustable height in order to limit the detection volume so that single particles are counted. The scattered light passes through an interference filter (width 0.1 nm) on to a photomultiplier. The multiplier signal is analyzed on line with a multichannel analyzer (MCA = Le Croy QVT 3001), in which the maximum value of the pulse is stored. The photomultiplier signal is matched to the MCA with a custom-built amplifier that has a high dynamic range (1 mV–10 V) and high bandwidth (0–500 kHz).

Since the Gaussian shape of the laser beam inhibits an accurate measurement of particle sizes, a trigger beam with a waist of 0.5 mm is placed just in front of the sizing beam. From the signal of this trigger beam a gate signal is derived for the MCA with a duration of 6 μs. During this gate period the MCA measures the signal of the particle going through the center of the sizing beam. The variation in the intensity of this part of the sizing beam is now less than 20%, so the intensity of the scattered signal is a measure for the particle size. The particle density is obtained from the number of pulses counted and the size of the scattering volume. The experimental setup has been calibrated with alumina particles which have diameters between 40–100 μm. These results have been extrapolated to particle sizes of 1 μm. The experimental uncertainty in the particle size then amounts to 100%. This value is also the limit of the proportionality of particle surface and the intensity of the scattered signal.[9]

Mass Spectrometer

Molecular impurities in the gas flow can be determined by analyzing the argon gas with a mass spectrometer. A stagna-

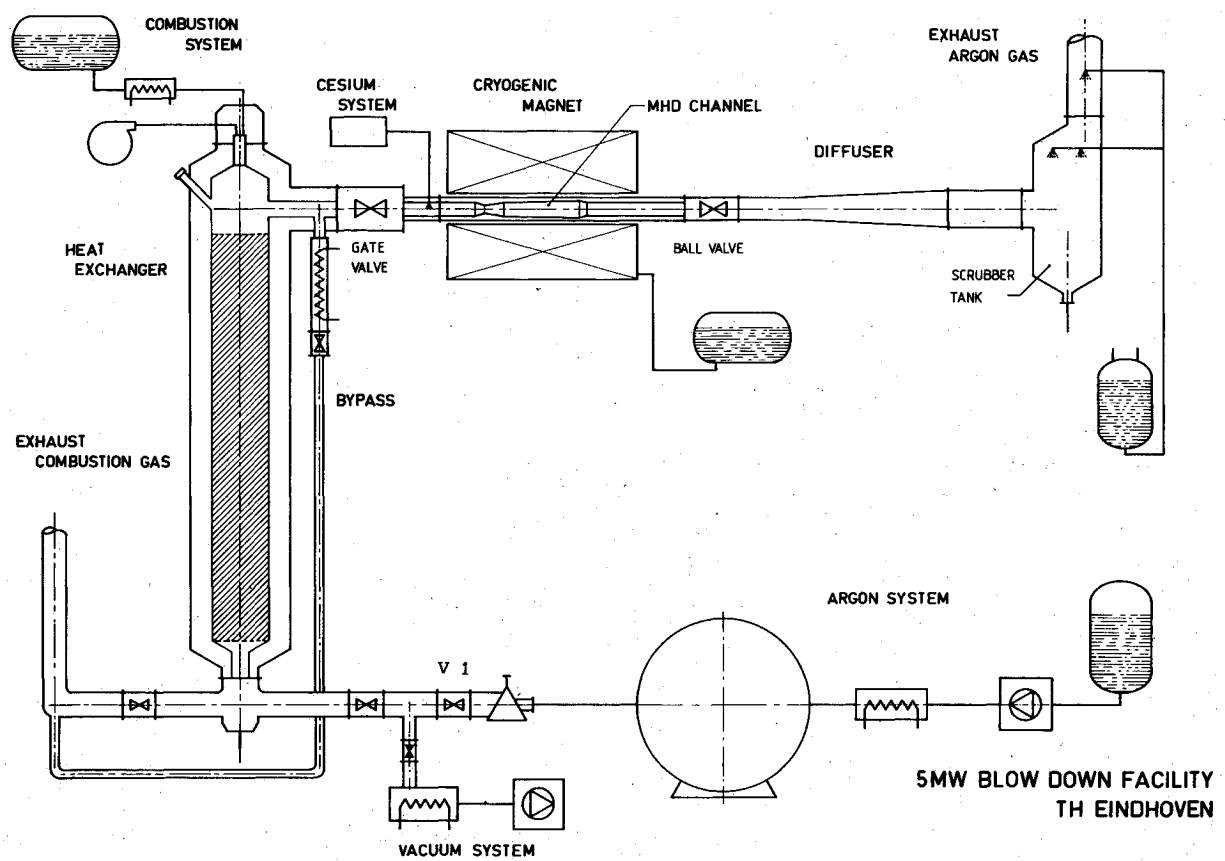

Fig. 1 Line diagram of the blowdown facility.

tion probe is placed in the supersonic diffuser just upstream of the ball valve. The gas is sampled in an ultra-high-vacuum recipient with a minimum pressure of 2.10^{-7} Pa applying a non-demixing gas inlet system (Balzers GES 010). A capillary tube of 4 m in length connects the mass spectrometer to the diffuser. This tube is kept at a temperature above 373 K to prevent condensation of water. The flow through the capillary tube is laminar and its time response is approximately 2 s.

The analysis is performed with a quadrupole mass spectrometer (Balzers QMG 101) coupled to a QMA 141 analyzer. Four mass numbers are measured with a frequency of 4 Hz. These numbers are 17, 28, 36, and 44, so the concentrations of water, nitrogen, and carbon dioxide are determined. It is also possible to scan the mass spectrometer to search for other contaminations. From calibration measurements the following detection limits were obtained: H_2O 40 ppm, N_2 10 ppm, and CO_2 10 ppm.

Absorption Measurement

The density of cesium atoms in the ground state in the MHD generator is measured using an absorption technique in the near wing of a resonance transition. The results were compared with the values obtained from the injected mass of cesium from the storage system.

The absorption measurements in the wings of the resonance lines are complicated by the broadening mechanisms that determine the shape of the wings. The impact theory will no longer hold for the wings and the quasistatic theory has to be used.[10] Two different wing regions can be distinguished. The first is the near wing, where the spectrum is determined exclusively by the interatomic difference potential of the radiating and perturbing atom. This van der Waals interaction potential leads to wavelength dependence with a power of -1.5, which has been observed in the red wings of many foreign gas-broadened lines. The second is the far wing, where the spectrum, in general, depends on the gas temperature. An increasing far red-wing intensity is observed in cesium gases as the gas temperatures increase,[11] whereas an opposite temperature dependency is observed in the blue wing. This can be explained by the respective attractive and repulsive, interatomic potential of the alkali-noble gas molecule.

From these considerations, it is evident that near-wing measurements are preferred for diagnostical purposes. The argon-broadened cesium resonance profiles, measured by Chen and Phelps,[10] therefore suggest that preferably the red wings of the 894.4- and 852.1-nm lines should be used.

For an optimal signal-to-noise ratio in the experiment the absorption should be approximately 50%. This would give a wavelength shift of 2.7 nm, according to the coefficients produced by Chen and Phelps[10] and the cesium density calculated from its injection rate (assuming a homogeneous filling of the channel). The measurements showed a bending of the absorption profile for wavelength shifts larger than 2.0 nm, indicating that the far wing region had begun. This leads to a small systematic error in the measurement because the temperature in the MHD generator is higher than the temperature in the MHD generator is higher than the temperatures used by Chen and Phelps[10] in their measurements.

Values of the argon density and the width of the cesium column are needed in order to calculate the cesium density. In the experiment, the argon density was obtained from gasdynamic calculations. However, this density increases during power extraction; therefore, the absorption measurement is performed at the beginning of the duct where the increase was less than 10% (see pressure measurements) and where it could be neglected in relation to other errors.

Spectroscopy

Recombination Radiation

Radiative recombination occurs when a free electron and an ion recombine to form a neutral atom. The excess energy from this reaction is released as a photon. The spectrum of the continuum emission arising from this process stops at the wavelength corresponding to the binding energy of the electron. The radiative power of this process varies quadratically with the electron density and linearly with the cross section of the process and with the electron energy distribution function.[12] Theoretically, a Maxwellian electron distribution function is assumed; the validity of this assumption was verified for argon cesium plasmas.[13] Argon and cesium ions contribute

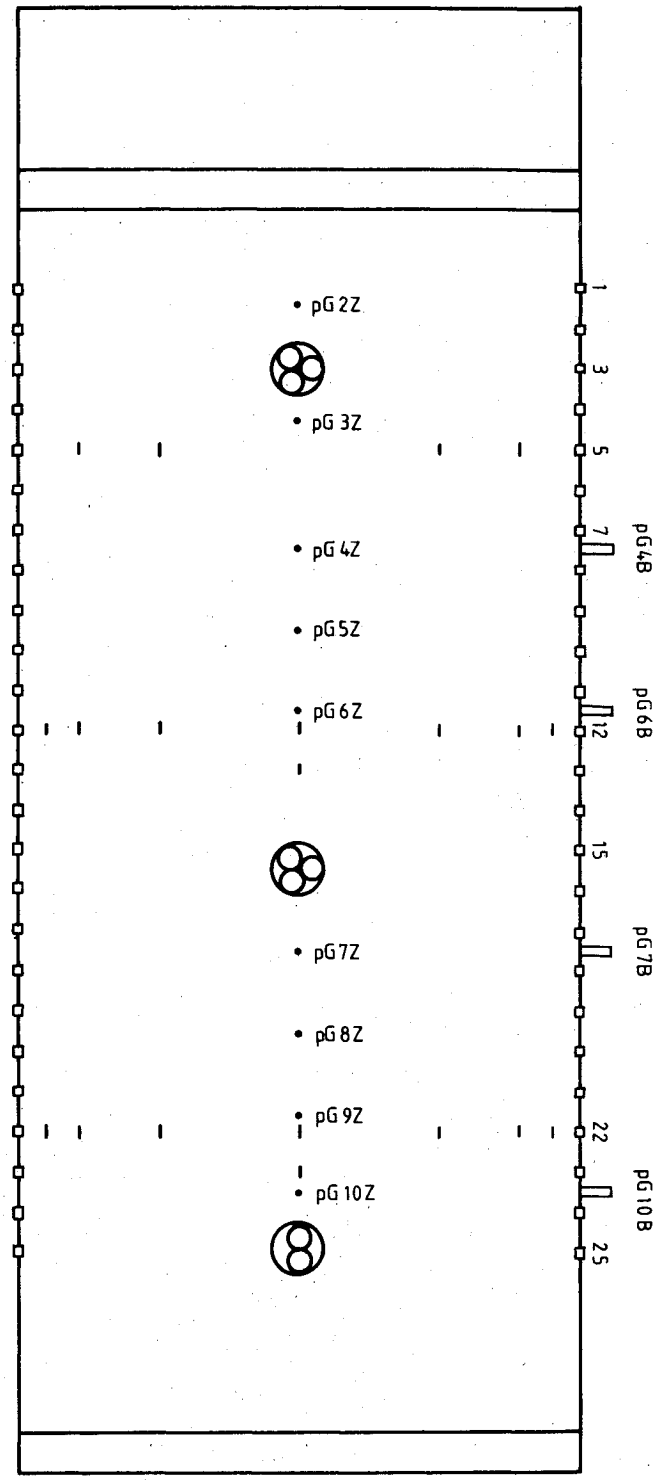

Fig. 2 View of a sidewall of the generator duct showing the positions of various diagnosis points: electrodes, (□); probes, (-); pressure transducers, (●); and the optical windows. In the windows, the lenses used with the fibers are drawn. The length of the channel is 824 mm and the electrode pitch is 28 mm. Electrodes measured with high frequency are 3, 15, and 25. The upper pressure transducers were sampled with 10 kHz, the sidewall transducers with 1 kHz.

to the emission in the same wavelength region but their intensities were shown to be orders of magnitude lower.[12] Since the recombination cross section had been measured[14] it was possible to derive the electron density from absolute intensity measurements. The ratio of two recombination radiation intensities at different wavelengths gave the electron temperature. An analysis of this method, however, showed that its accuracy rapidly decreased at temperatures above 4000 K.[12]

Line Emission

Line emission originates from the spontaneous transition of an atom from an excited state to a lower state. If the absolute emissivity is measured and the oscillator strength of the transition is known, then the density of the upper level can be calculated. From this density it can be concluded whether or not the discharge is in local thermal equilibrium (LTE). According to Ref. 1, the electron temperature may be higher than the gas temperature, so LTE is not attained. Therefore, this measurement gives important information about the actual situation inside the plasma of the generator. In calculations, partial LTE (PLTE) is sometimes assumed and this appears to be valid for evaluating the aforementioned parameters.[7,13]

The measured line intensity also can be used to determine the electron temperature from the line-to-continuum ratio.[15] Likewise, this method is based on the assumption of PLTE. This method was found to be more sensitive to variations in the electron temperature from the analytical point of view than the relative continuum intensity method.[16] Another advantage of this method was that the temperatures were less dependent on the electron density. In Ref. 17, it is shown that a 50% density deviation only gave a 2% temperature error.

Electrical Measurements

Low-frequency measurements (4 Hz) were performed for all electrode voltages and the generated power was calculated from them. The floating potential of various electrodes was measured in order to obtain the Hall voltage that builds up in the direction of the flow. Probes were fitted in the sidewall flush with the insulator wall in order to measure the cathode and anode voltage drops as well as the average electrical field across the height of the duct. Subsequently, this could be used for calculating an average electrical conductivity.

Some signals also were recorded on an Ampex analog tape recorder with a bandwidth of 500 kHz, which was fast enough to obtain data from individual streamers. The voltages of three electrodes—one Hall voltage, six signals from photomultipliers, and two pressure signals—were recorded with this instrument.

Pressure Measurements

When making the first measurements[8] it was observed that in the duct and in the supersonic diffuser the pressure was much higher than expected from gasdynamic calculations. This reduced the gas velocity and limited the power extraction. Another problem was the fracture of ceramic plates inside the duct, which indicated large pressure variations producing severe mechanical loads on the walls. High-frequency pressure transducers were installed in order to measure these pressure variations when recording measurement series 6 and 7. Piezoresistive transducers with a resonance frequency of >20 kHz were used (Kistler) but the frequency response was limited to 1 kHz in measurement series 6, due to the length of the tube that connects the transducer to the duct. In series 7 this was upgraded to 10 kHz.

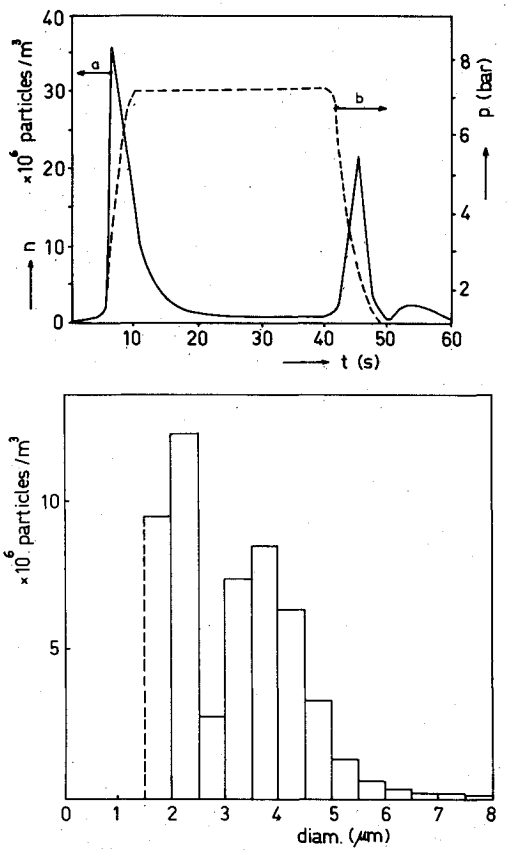

Fig. 3 a) Particle concentration (a) during run 105. The stagnation pressure (b) is plotted for comparative purposes. b) Particle diameter concentration during stationary flow in run 107.

Table 1 Some parameters of the runs when significant power was extracted[a]

Run	T_{stag}, K	P_{stag}, bar	Mass flow, kg/s	B_{max}, T	R_{load}, ohm	Cesium, %	P_{th}, kW	$P_{e,m}$, kW
202	1900	7.2	5.0	5.2	6.0	0.05	4930	190
204	1870	7.2	5.0	5.3	6.0	0.04	4850	270
205	1910	7.2	5.0	5.3	4.0	0.05	4960	286
302	1910	7.4	5.2	5.2	9.0	0.10	5155	230
303	1900	7.4	5.1	5.1	6.0	0.14	5030	362
402	1910	7.0	4.9	5.0	6.0	0.15	4800	0.7
502	1890	7.4	5.1	5.0	6.0	0.12	5120	56
603	1950	7.3	5.0	5.0	6.0	0.10	5060	31
702	1920	7.2	5.0	5.2	5.6	0.11	4970	393
703	1910	7.2	5.0	5.1	5.6	0.12	4950	423
704	1890	7.2	5.0	5.3	7.3	0.14	4900	300

[a] T_{stag} = stagnation temperature; P_{stag} = stagnation pressure; B_{max} = maximum magnetic induction; R_{load} = load resistance; Cesium = amount of cesium injected compared to the mass flow; P_{th} = thermal input power; $P_{e,m}$ = *electrical output power at maximum magnetic induction.*

Figure 2 is a diagram of a sidewall of the duct showing the positions of the measurements with the positions of electrodes, probes, pressure transducers, and optical windows. For measurement series 2–6, the light from the windows was guided through prisms and lenses; later, they were replaced by optical fibers made of quartz. Lenses with a diameter of 12 mm and a focal length of 8 mm were mounted on the sidewall of the duct in order to focus the light into the fibers. Because of this small size the setup was very rigid and insensitive to vibrations of the wall; furthermore, three lenses were placed behind each window. Other advantages were that the system had fewer optical components so it was easier to set up, the transmission loss of the fibers was 100 times lower than that of the lens system, and the photomultipliers could be located farther away from the magnet (25 m). Similar optical windows were fitted in the other sidewall, but without probes or pressure transducers. Argon was blown on the cold windows in order to prevent contact with cesium; however, this was insufficient and the transparancy of the windows had to be measured with a He-Ne laser.

Photography

A window was made in the scubber tank in order to inspect the channel, which also gave an opportunity to observe the plasma in the generator during the power extraction and to record it on video. Two cameras were used with different sensitivities in order to record inside the duct with and without streamers. A high-speed camera was used (up to 8000 frames/s) to observe individual streamers. An Imacon camera was available to make streak or framing pictures, but restricted access to the channel made it difficult to obtain good results with this camera.

IV. Experimental Program

Experiments with the blowdown installation were performed in series of measurements; one run per 24 h could be achieved due to the time required for warming up the heat exchanger and because the magnet had to be operated at night. Each measurement series consisted of several runs on consecutive days. All of the runs were numbered. In 1981, series 1 was run with the purpose of testing the heat exchanger. The maximum stagnation temperature of the argon gas was 1970 K, and it was attained after seven runs. In series 2, the complete process was tested. Some important parameters of runs are listed in Table 1 when significant power was extracted.

Since problems occurred with the boron nitride walls of the duct and the supersonic diffuser, the duct walls were made of reaction bonded silicon nitride during series 3. The first four electrodes were short-circuited in order to improve ionization in the inlet region; currents in excess of 200 A were measured at these electrodes and, after three runs, severe damage to the duct was observed. The diffuser was damaged as well. During series 4 and 5 another duct was tested with a preheat loop installed. Malfunctioning of the cooling panels resulted in water leakage. It was concluded that, with the installed preheat loop, the necessary low contamination level could not be attained. In series 6, the channel used for series 3 was rebuilt with boron nitride walls but again problems occurred and the power output was limited (see Table 1). After this series, a new channel was built with different inner walls and a completely new concept for the supersonic diffuser. The channel walls were made of silicon nitride and the diffuser was made of small tiles using a new type of boron nitride (HDBN). Details of the wall constructions will be published in a separate article. This channel and diffuser were tested during the five runs of series 7. Run 701 was used for cleaning the channel by baking it. No damage was found except in one case where a definite fault was found. This is discussed in Sec. 5. Now the hot flow train seems to be in good working order, ready for further experiments.

V. Results of Diagnosis

Dust Loading

The most important results obtained for the dust loading measurements during the first blowdown experiments (series 1) are presented in Figs. 3a and 3b. They show the concentration against time (3a) and the diameter distribution function of the particles (3b) at stationary flow conditions. Fig. 3a shows a marked increase in the concentration as the flow starts, followed by a sharp decrease just before a steady flow is reached. A fairly constant concentration of about 2 particles

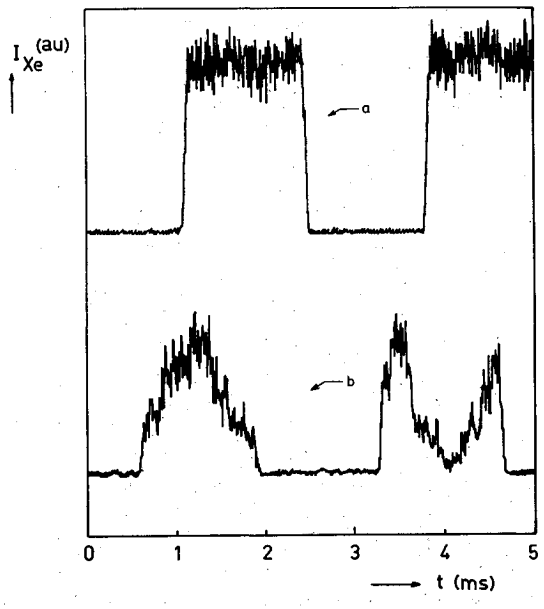

Fig. 4 Signal of the absorption measurement recorded with the Ampex. The upper trace (a) is taken before cesium is added, the lower (b) is with cesium but before power extraction.

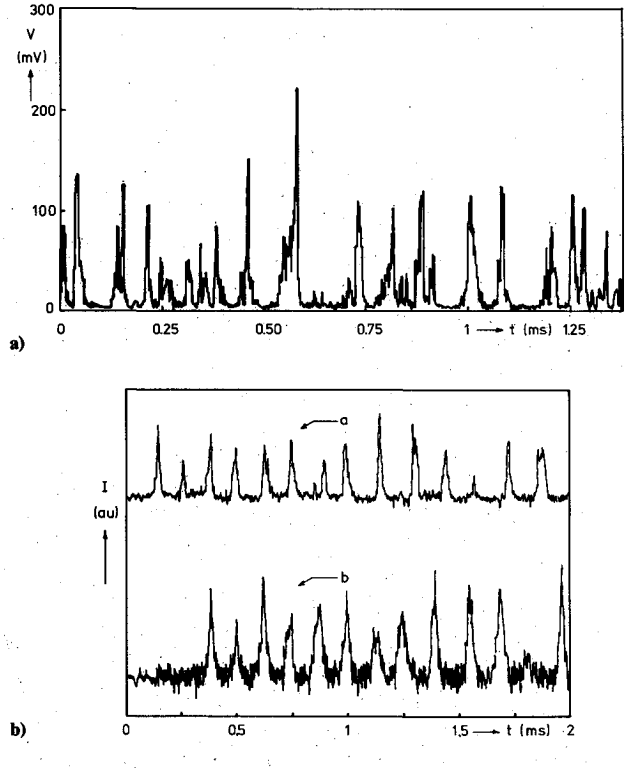

Fig. 5 a) Typical example of a recombination radiation signal during run 302 in the center of the channel (490 nm). b) Typical example of a line radiation signal (723 nm) during run 702 in the center (a) and the end (b) of the channel.

per cm^{-3} is reached after 3 s of steady flow. This is the time the gas needs to pass the whole heat exchanger. When the run terminated a sharp peak appeared again due to depressurization of the heat exchanger. These results are in agreement with those of previous experiments by Cook,[3] although a different technique was used with a similar type of heat exchanger.

In Table 2, the particle concentration during a steady flow is shown for different runs. It can be observed that the particle concentration varies considerably from run to run, mainly due to corroding effects on the generator. It must be stated that for particle concentrations up to 300 particles per cm^3 no correlation with the power extracted was found. After series 4, the Mie scattering was no longer used. Its main function had been to check the heat exchanger; however, since this exchanger gave no problems and had a very low dust density, the extra effort needed for this part of the experiment was removed.

Molecular Contaminations

The densities of H_2O, N_2, and CO_2 were measured with a mass spectrometer. It was seen that when the flow started a sharp decrease in contamination appeared, probably because the residual combustion products were immediately carried away. Most impurities occurred 3 s after the stationary flow condition was reached; this can be explained by the degassing of the system, especially the ceramics. Table 2 shows the impurity levels for several runs during power extraction. Usually the impurities were acceptably low but during run 303 the N_2 density increased slightly, probably as a result of arcing across the electrode pairs 3 and 4 which attacked the silicon nitride walls. No effect of this was seen on the extracted power.

In runs 401 and 402, contaminations were very high due to the malfunctioning of a cooling panel in the duct wall. While extracting power the concentrations of water and nitrogen in the gas were more than 3500 and 2000 ppm, respectively. The high level of water in combination with the heat of the argon gas resulted in flaking of the boron nitride inner walls of the generator duct. The mean power extracted during these two runs was 0.8 kW; however, from an analysis of the high-frequency electrode currents and the radiation signals, it was observed that a good power generation was obtained for short time intervals (0.5 ms). This suggests that the generator either works well or it does not work at all when the circumstances are unfavorable. The same fluctuating power outputs were measured during series 5 and 6.

Cesium Density

For series 2–6, the absorption measurement was carried out at the 894.4-nm resonance line from cesium. During series 6 and 7, the measurement was performed at the upstream end of the channel but for the other series it was performed in the center. The results are presented in Table 2. A large discrepancy always occurred between the amount of cesium injected (from which an average density could be calculated) and the measured amount. Several improvements to the injection system reduced this difference, although it remained. After series 6 an experiment with an oven was performed in order to search for possible errors and it was discovered that much of the error came from the xenon light source. This source had a line at 895 nm and the absorption measurement was carried out on the wing of this line, which makes the measurement very sensitive to errors in wavelength shift. In the experiment, it was found that results obtained in the wing of the 852.2-nm cesium line were up to ten times more accurate. In this wavelength region the xenon lamp had a very constant output. The overall accuracy of this experiment is 5%, most of the remaining error due to inaccuracy of the oven temperature. During series 7 the remaining discrepancy was 30%; this can be explained by imperfect mixing.

The absorption measurement signal showed an unexpected behavior when recorded at high speed with the Ampex recorder. Considerable fluctuation was observed. An example of this effect is shown in Fig. 4. The upper trace is the signal of the xenon lamp before cesium is added. The lower trace is measured with cesium injection, but before the power extraction since the emission of the streamer then dominates the signal. The amplitude variations were up to a factor of four. The frequency of these fluctuations is always in the order of 1 kHz. Up to now the cause is uncertain and there is no indication that the power extraction has the same fluctuations. This will be investigated further by performing a Fourier analysis of the signals that were recorded with the Ampex.

Electron Density and Temperature

The electron temperature has been determined from the relative intensities; therefore, no information about the streamer structure is needed. The temperatures can be obtained from the time integrated data (0.25 s) recorded with a 176-channel multiplexed ADC (DGDAC) which records the low-frequency signals. The resultant temperature was slightly more than 4000 K for the whole power extraction. This was measured in the center of the channel and was identical with the other runs. Also near the entrance a constant temperature was found which had a value of approximately 3000 K, although this value was rather uncertain due to calibration problems.

Measurements of the radiation with high time resolution gave much information on the streamer structure in the bulk of the generator.[18] Figure 5 shows two examples of line radiation signals. A large difference occurred between series 2–6 and series 7. Figure 5a is from run 302, Fig. 5b from run 702. During the first series, the streamer pattern was quite irregular. The results of series 7 are far more regular and with an autocorrelation technique a well-defined streamer fre-

Table 2 Various diagnoses[a]

Run	H_2O, ppm	N_2, ppm	CO_2, ppm	$10^6 m^{-3}$ Max	Dust, Min	Cs, $10^{21} m^{-3}$	Cs-rel	n_e, $10^{21} m^{-3}$
202	—	—	—	>320	20	1.9	7.0	3.2
204	60	25	30	>140	10	—	—	—
205	60	60	20	>160	30	—	—	—
302	50	80	—	260	35	4.2	4.3	2.9
303	50	300	—	240	300	—	—	—
402	3500	—	—	>200	200	5.7	3.0	4.0
502	40	125	—	—	—	4.6	3.6	3.5
603	300	50	30	—	—	3.8	2.9	4.0
702	150	100	20	—	—	1.4	1.3	—
703	125	100	20	—	—	1.5	1.3	—
704	700	100	30	—	—	1.8	1.3	—

[a] H_2O = maximum amount of water during power extraction; N_2 = maximum amount of nitrogen; CO_2 = maximum amount of carbon dioxide; dust = particle density during stationary flow; Cs = cesium density measured by the absorption method; Cs-rel = ratio of cesium density by the absorption method and by the injected amount; n_e = average measured electron density.

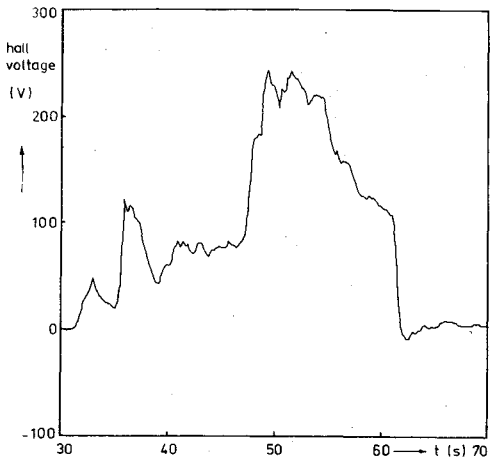

Fig. 6 Hall voltage between electrodes 1 and 25 for run 702.

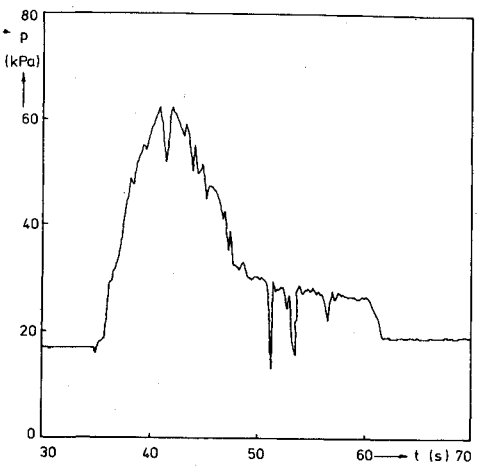

Fig. 7 Pressure distribution in the supersonic diffuser for run 702.

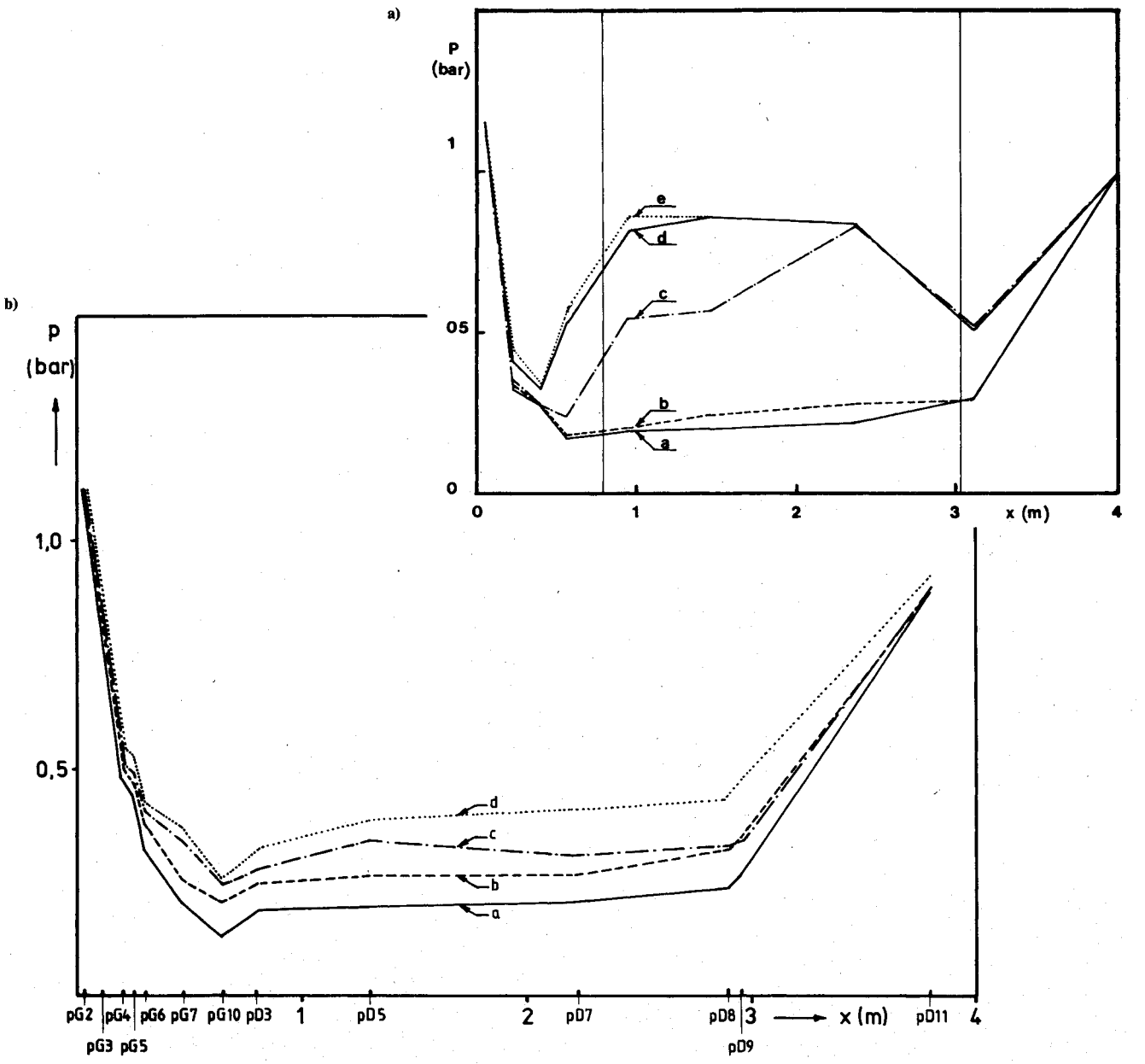

Fig. 8 a) Static pressure distribution in the hot flow train at increasing B field during run 302; a) B = 0 T, b) B = 3.6 T, c) B = 4.1 T, d) B = 4.6 T, and e) B = 4.7 T. b) Static pressure distribution during run 703; a) B = 0 T, b) B = 3.6 T, c) B = 4.2 T, and d) B = 5.2 T.

quency could be found at 10 kHz. From cross-correlation determinations the streamer velocity was found to be 1050 ± 50 m/s. The detailed results from the correlation analysis will be treated in a subsequent article.

The line-to-continuum method was used to determine the electron temperature during runs 602 and 603. The results were compared to those of the relative continuum method that had been used up to that time. It was found that the spread in the results was reduced by half. The final result obtained with the line-to-continuum method was 4500 ± 500 K in the center and end of the channel and 4000 ± 700 K at the beginning, confirming the impression that the electron temperature is slightly lower at the entrance than farther downstream.

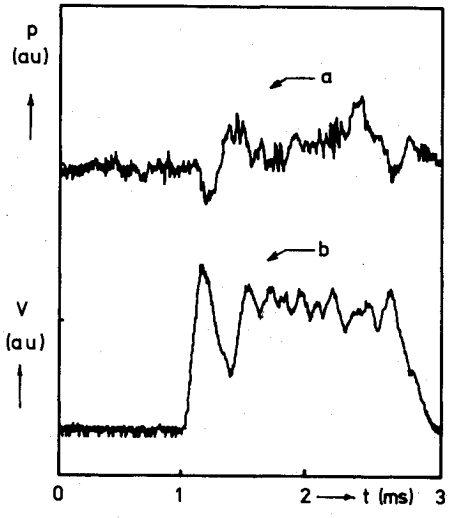

Fig. 9 Voltage of electrode 25 (a) and pressure PG10B (b) at the end of the channel during run 704.

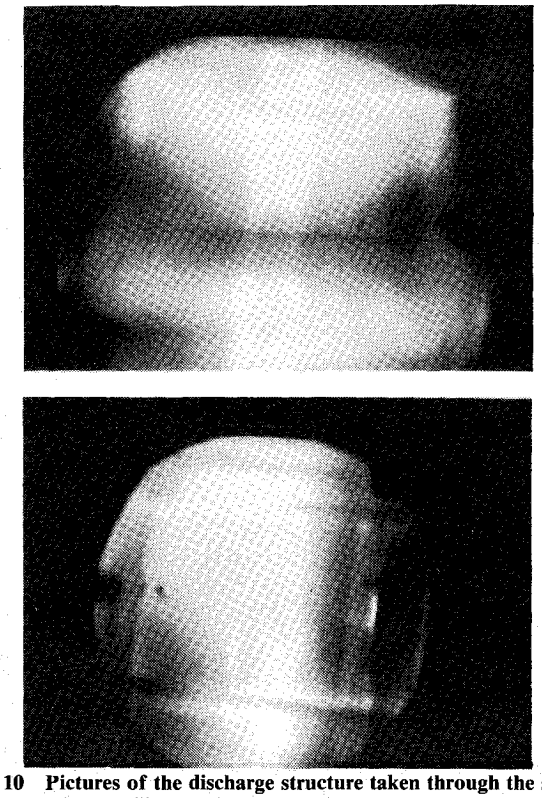

a)

b)

Fig. 10 Pictures of the discharge structure taken through the scrubber tank: a) run 603, the discharges in the upper corners are in the stainless steel supersonic diffuser; b) run 702, at the top, the discharge fills the channel width; at the bottom, only a part of the electrode is covered. In the right sidewall the discharge in the window opening is seen (see Sec. 5).

High-Frequency Electrode and Probe Voltages

During series 4, 5, and 6, the generator worked only for short periods, appearing to be just at the threshold of ignition. For series 4, the presence of water contributed to this malfunctioning but this could not explain the problems in the other series. Another reason for the bad ignition conditions was suggested by the high-frequency electrical data because a time lag of 0.1 ms was seen between the voltage and current of one electrode pair. This time lag is caused by the self-inductance of the coil-shaped load resistors. During this time lag the streamer moved about 10 cm through the channel but the current could not follow this speed. This problem was less pronounced in series 2 and 3 because the first four electrodes were short-circuited and the second four electrodes were connected to a different type of resistor with low inductance.

After series 6 the load resistors were replaced by resistors with a very low self inductance. For series 7 the voltage and current signals of the electrodes were in phase. As can be seen in Fig. 5b the streamer pattern there was very regular, indicating that the ignition conditions were then good despite the considerable amount of water present during runs 704 and 705.

The voltage of the probes in the sidewall were recorded with the 4-Hz DGDAC system; from this data, the cathode and anode voltage drops can be calculated. The average field in the bulk was used to calculate the average conductivity of the plasma. The maximum value was 6 mho/m obtained during run 302 and for run 603 it was 1.3 mho/m. A log-log plot of the conductivity vs the current density gives a straight line with a slope of 1.25 for run 302 and 0.99 for run 603.

Pressure

An unwanted event that occurred during run 702 gave very useful information about the pressure inside the generator. A short circuit at the end window of the generator (see Fig. 2) produced a Hall current through the channel. It was seen over the Hall voltage across the whole channel (Fig. 6) and it affected the pressure inside the supersonic diffuser (Fig. 7).

A Hall shorting leads to an increase of the pressure downstream. In previous runs, this increased pressure had been observed although it could not be explained. Now, this increase in pressure can be attributed to the stainless steel part of the supersonic diffuser inside the magnet. It produced a large Hall shorting accompanied by a pressure increase. In series 7, the stainless steel part has been replaced by a ceramic one and the influence of insulating it can be seen in Fig. 8 where the pressures in the hot flow train for runs 302 and 703 are plotted. The pressures for run 703 were almost identical to those for the quasi-one-dimensional gasdynamic calculations. The low pressure observed in series 7 is useful because it indicated that a higher power extraction was still possible.

Two Kistler pressure signals were recorded with the Ampex tape recorder. The time resolution of this signal was limited by the transducer and its connecting tube; however, with this device, it was still possible to measure individual streamers. An example is shown in Fig. 9. It can be seen that, when a streamer passes, the pressure drops and then, after some 0.1 ms, it rises above the initial value. The analysis of these signals will be discussed in a subsequent article.

Photography

Pictures taken from the video recording during runs 603 and 702 show differences in discharge structure between the use of a stainless-steel diffuser and an insulating one (Fig. 10). During run 603 the discharges are seen in the corners of the diffuser (Fig. 10a). This is the Hall shorting which causes the high pressure in the diffuser and in the channel. The picture of run 702 (Fig. 10b) shows the discharge only at the sidewall at the moment the short circuiting to the end window occurs. In the corners of the diffuser, there is no longer discharge.

VI. Remarks and Conclusions

Over the past five years a vast amount of information has been obtained about the performance of a closed-cycle MHD generator. Emphasis should be laid on those measurements that specifically deal with the features of the closed cycle. Some important parameters that have been measured in this respect are the dust loading, the amount of impurities, the seed fraction, the electron temperatures and densities, the streamer velocities, and the pressure fluctuations.

Dust loading was measured with Mie-scattering equipment. Its main purpose was to check the amount of dust coming from the heat exchanger. The amount of dust measured was low (about $2*10^8$ m^{-3}) but no influence on the power extracted was examined. When a ceramic plate of the channel wall collapsed, this could be seen clearly as an increased dust density recording.

The amount of molecular contaminations has to be low in a closed-cycle generator; to check this impurities were measured using a quadrupole mass spectrometer. During power extraction, three molecules were monitored: H_2O, N_2, and CO_2. When the channel was vacuum sealed the molecular densities fell below their maximum permitted values. When the first run of a measurement series was used to clean the channel, the impurities were low enough for a good generator performance. In series 2, 3, and 7, this cleanup was done with good results. In series 4 problems with cooling water panels led to high water contamination. In series 5 and 6 the importance of the cleaning was overlooked, resulting in a very low power output and a fluctuating generator behavior.

The seed fraction is always important in MHD generators and it can be measured in two ways, by measuring the amount of seed injected or using an optical absorption method. Originally these methods did not give identical results but imperfect mixing could have been the reason. From some test measurements in an oven, it was found that the xenon light source introduced an unexpected error in the measurement. Since the 894-nm resonance line was in the neighborhood of a xenon line, the results were very sensitive to errors in the wavelength shift. Using the 852-nm line instead, where the light source had a constant output, the error of the cesium density measured was reduced by a factor of ten in the oven experiment. The final accuracy obtained was 5%. With the 852-nm line, the difference between the injected and measured cesium density in the generator during the measurement series 7 was reduced to 30%. This difference can be ascribed to residual experimental errors or imperfect mixing of the cesium and argon.

Electron temperatures are of specific interest in the closed-cycle generator, since this is one of the most important differences between it and the open-cycle generator. The electron temperature in a closed-cycle generator can be much higher than the gas temperature. Therefore, the temperature of operation can be lower than in the case of the open cycle, where the electron and gas temperature are equal. The electron temperature was measured optically, using a continuum ratio or a line-to-continuum ratio. Both gave an average temperature of 4500 K. The second method had a lower experimental error: 1000 against 500 K. In the inlet region, the temperature was slightly lower; 4000 ± 700 K was found with the line-to-continuum method.

The electron density inside the streamer was measured from the absolute intensity of recombination radiation and the average value obtained was $(3.5 \pm 2.0)*10^{21}$ m^{-3}. This indicates that the seed is almost completely ionized.

The channel velocities can be obtained by measuring signals at different positions with the aid of optical signals. The streamer velocity was 1050 ± 50 m/s. The gas velocity calculated from a gasdynamics model was 1200 m/s, but the gas slowed down during the interaction.

Pressure fluctuations could be seen during the power extraction. The effects of individual streamers were seen with high-frequency probes. From pressure measurements in the diffuser it was seen that Hall shorting in the generator gave a marked pressure increase so avoiding this shorting was essential in order to reach the maximum power output. This was achieved by using ceramic walls inside the whole magnet in series 7. The results of the pressure distribution along the hot flow train indicate that an even greater power output could be achieved.

High-frequency measurements of electrode voltage and current showed a time lag of the current in series 2–6. This was due to the self inductance of the load resistors. After fitting resistors with a very low inductance in series 7 the streamer pattern became much more regular, which indicated that the ignition conditions were better, probably because a current could start to flow more easily.

The most important conclusions to be drawn from this work are that a closed-cycle MHD generator will work well when the hot flow train inside the magnet does not contain any metal parts except for the electrodes, when molecular contaminations do not exceed 100 ppm, and when the load resistors have a low inductance. The experimental results presented here will help to design a theoretic model of a closed-cycle MHD generator which can lead to a better understanding of its functioning and further optimization of its performance.

Acknowledgments

This work was performed with financial support from the Netherlands Department of Economic Affairs and the Stichting voor de Technische Wetenschappen (STW). The authors wish to thank L. H. T. Rietjens, J. Uhlenbusch, J. W. M. A. Blom, and A. Veefkind for their cooperation. The authors also acknowledge the valuable contributions of J. P. van Dijke, A. P. C. Holten, H. F. Linders, J. T. W. J. Nouwen, and C. H. F. M. van de Weem.

References

[1]Kerrebrock, J. L., "Non-equilibrium Ionization Due to Electron Heating: I. Theory," *AIAA Journal*, Vol. 2, June 1964, pp. 1072–1080.

[2]Zlatanovic, M., Veefkind, A., and Rietjens, L. H. Th., "Performance of a Closed-Cycle MHD Generator with Molecular Impurities," *Journal of Energy*, Vol. 3, Jan.–Feb. 1979, pp. 23–29.

[3]Cook, C. S. and Dickinson, K. M., "Argon Contamination Associated with Regenerative Heat Exchanger for Closed-Cycle MHD," *Proceedings of the 16th Symposium on Engineering Aspects of MHD*, Paper II.4, Pittsburgh, PA, 1977, pp. 22-30.

[4]Tate, E, Marston, C. H., and Zauderer, B., "Large Enthalpy Extraction Experiments in a Non-Equilibrium Magnetohydrodynamic Generator," *Applied Physics Letters*, Vol. 25(10), Nov. 1974, pp. 551–553.

[5]Veefkind, A., Houben, J.W.M.A., Blom, J. H., and Rietjens, L.H.Th., "High Power Density Experiments in a Shock-Tunnel MHD Generator," *AIAA Journal*, Vol. 14, Aug. 1976, pp. 1118–1122.

[6]Self, S. A. and Kruger, C. H., "Diagnostic Methods in Combustion MHD Flows," *Journal of Energy*, Vol. 1, Jan. 1977, pp. 25–43.

[7]Flinsenberg, H. J., "Fossil Fuel Fired Closed-Cycle MHD Power Generating Experiments," Thesis, Eindhoven University of Technology, 1983.

[8]Massee, P., "Gasdynamic Performance in Relation to the Power Extraction of an MHD Generator," Thesis, Eindhoven University of Technology, 1983.

[9]Kerker, M., The Scattering of Light and other Electromagnetic Radiation, Academic Press, Orlando, FL, 1969.

[10]Chen, C. L. and Phelps, A. V., "Absorption Coefficients for the Wings of the First Two Resonance Doublets of Cesium Broadened by Argon," *Physical Review A*, Vol. 7, 1973, pp. 470–479.

[11]Behmenburg, W., "Line Shapes," *Progress in Atomic Spectroscopy*, Part B, edited by W. Hanle and H. Kleinpoppen, Plenum, New York, 1979, pp. 1187–1226.

[12]Wetzer, J. M., "Electron Density Determination in Ar-Cs Plasmas," *Physica*, Vol. 123C, 1984, pp. 247–256.

[13]Borghi, C. A., "Discharges in the Inlet Region of a Noble Gas MHD Generator," Thesis, Eindhoven University of Technology, Eindhoven, the Netherlands, 1982.

[14]Norcross, D. W. and Stone, P. M., "Radiative Recombination in Cesium," *Journal of Quantum Spectroscopy and Radiative Transfer*, Vol. 6, 1966, pp. 277–290.

[15]Cabannes, F. and Chapelle, J., "Spectroscopic Plasma Diagnostics," *Reactions under Plasma Conditions*, edited by M. Venogupalan, Wiley, New York, pp. 367–466.

[16]Wetzer, J. M., "Spatially Resolved Determination of Plasma Parameters of a Noble Gas Linear MHD Generator," Thesis, Eindhoven University of Technology, 1984.

[17]Vaessen, P.H.M., "Heat and Momentum Transfer from an Atmospheric Argon Hydrogen Plasma Jet to Spherical Particles," Thesis, Eindhoven University of Technology, 1984.

[18]Sens, A.F.C., Bityurin, V. A., Wetzer, J. M., Veefkind, A., and Bravers, J.F.G., "Investigations of the Gasdynamical Effects of a Non-equilbrium Supersonic Flow with Streamers in a Noble Gas MHD generator," *20th Symposium on Engineering Aspects of MHD*, Irvine, CA, 1982, pp. 10.6.1–10.6.7.